

Dynamical generation of scalar mass in two Higgs doublet model under Yukawa interactions

Tajdar Mufti *

Lahore University of Management Sciences
Opposite Sector U, D.H.A, Lahore Cantt., 54792, Pakistan

July 8, 2025

Abstract

Light scalars are among the expected particles in nature. If they indeed exist, dynamical generation of masses becomes an important phenomenon to investigate in scalar interactions. A two Higgs doublet model containing two complex doublet scalar fields, conveniently called the standard model Higgs and the second Higgs fields, is studied to explore the extent of dynamical mass generation and the field propagators in the model at different cutoff values. Both Higgs fields are coupled with each other by a real singlet scalar field through a modelled Yukawa interaction. The model is studied for various renormalized masses of the second Higgs field at various coupling strength. The renormalized mass of the standard model Higgs boson is kept at 125.09 GeV. The model has strong indication of existence of critical coupling below 10^{-3} GeV. The observed dynamical masses are generally within 200 MeV. The two Higgs propagators are found to be considerably stable compared to scalar singlet propagators despite cutoff effects. No phase structure in the parameter space was observed. The model is found non-trivial.

1 Introduction

Dynamical mass generation (DMG) [1–12] is a non-perturbative phenomenon by definition. Historically, it has mostly been relevant to QCD physics [13], particularly to the lightest family of quarks due to limited capacity of QCD interactions to generate large dynamical masses. In the new physics, the phenomenon is equally relevant to masses considerably lighter than the electroweak scale. As the existence of scalar sector in nature has become a

*tajdar.mufti@gmail.com, tajdar.mufti@lums.edu.pk

possibility after the experimental finding of the Higgs boson [14–18], ascertaining the extent of dynamical generation of scalar masses¹ due to different interactions [19–22, 22–26] can not be underestimated.

Yukawa interaction vertex is among the phenomenologically interesting vertices [27–29]. Despite that it is mostly considered in fermionic interactions, no unassailable argument exists to prohibit it in scalar sector. A model containing the vertex and the standard model (SM) Higgs field serves as an important avenue to explore the scalar sector. Two Higgs doublet models (2HDM) [30–32] are among the widely studied models. Relevant to scalar sector, a 2HDM presents two important scenarios once the SM Higgs [16, 17] is introduced in the theory. First, the model presents a mock up scenario of fermions interacting with the SM Higgs. Second, the model presents an opportunity to investigate how same particles from two different families interact with each other. A highly interesting aspect in both scenarios is that the physics of dark matter in scalar sector arising from possible Higgs-ultralight scalar ($m_s = O(10^{-22})$ eV) interactions [33–40] can also be studied in the model, though it may be more challenging in terms of controlling the involved numerics.

This paper is an extension of Wick Cutkosky (WC) model [41–45] to incorporate two complex doublet fields, termed as the SM Higgs, and the second Higgs fields² for convenience. The two Higgs fields interact with each other only by a real singlet scalar field. The aim is to study the role of Yukawa interaction³ in dynamical scalar mass generation in different regions of the parameter space of the model at different cutoff values, and extract a representative function of the dynamical mass. The renormalized⁴ masses of the two complex doublet scalars are kept at their physical masses in order to study the phenomenon of DMG from the perspective of phenomenology. The physical mass of the SM Higgs is kept at its experimentally known value [14] while the renormalized mass of the second Higgs is chosen for different scenarios mentioned above. A certain advantage of fixing masses is reduction of the parameter space to be explored. It greatly facilitates in training an algorithm [46], which is no longer a novel approach in quantum field theory [47–49], over the samples of calculated dynamical masses in different regions of the parameter space, the details are given in the next section. An advantage is that the quantities subject to training become readily available for richer field theory models which may involve larger Dyson Schwinger equations (DSEs) [50–54] which are more resource hungry.

The approach of DSEs is used for the study. The DSEs for the three field

¹In this paper, the dynamical mass is defined as the renormalized mass for numerically negligible bare mass.

²It has the same symmetry as the SM Higgs but different renormalized masses.

³The term is borrowed from the Yukawa interaction of fermions for convenience.

⁴The terms renormalized mass and physical mass are interchangeably used throughout the paper for the SM Higgs. The term scalar field is reserved only for the singlet scalar.

propagators are considered while the interaction vertices are fixed at their tree level form up to certain renormalization dependent terms, the details are given in the next section.

There exist other renormalizable vertices to further extend the model [27–29]. However, such richer models may require further truncations and ansatz [53] for the approach of DSEs. As strength of Yukawa vertices to produce dynamical mass is investigated, quartic interactions are not considered at this point.

2 Technical Details

The Euclidean version of the Lagrangian ⁵ with the counter terms is given by

$$\begin{aligned}
L = & \frac{1}{2}(1 + A)\partial_\mu\phi(x)\partial^\mu\phi(x) + \frac{1}{2}(m_s^2 + B)\phi^2(x) + (1 + \alpha)\partial_\mu h^\dagger(x)\partial^\mu h(x) \\
& + (m_h^2 + \beta)h^\dagger(x)h(x) + (1 + a)\partial_\mu H^\dagger(x)\partial^\mu H(x) + (m_H^2 + b)H^\dagger(x)H(x) \\
& + (\lambda_1 + C_1)\phi(x)h^\dagger(x)h(x) + (\lambda_2 + C_2)\phi(x)H^\dagger(x)H(x)
\end{aligned} \tag{1}$$

where A , B , α , β , a , b , C_1 , and C_2 are coefficients due to the counter terms in the Lagrangian. The real singlet scalar field is represented by $\phi(x)$, $h(x)$ is designated for the SM Higgs boson while $H(x)$ represents the second Higgs boson ⁶. The resulting DSEs for the field propagators are given below:

$$\begin{aligned}
D_h^{-1}(p) = & (1 + \alpha)p^2 + m_h^2(1 + \alpha) + 2(1 + A)(1 + \alpha)(1 + a)\sigma_h + \\
& (\lambda_1 + C_1) \int_{-\Lambda}^{\Lambda} \frac{d^4q}{(2\pi)^4} D_s(q) \Gamma_1(-p, q) D_h(q - p)
\end{aligned} \tag{2}$$

$$\begin{aligned}
D_H^{-1}(p) = & (1 + a)p^2 + m_H^2(1 + a) + 2(1 + A)(1 + \alpha)(1 + a)\sigma_H + \\
& (\lambda_2 + C_2) \int_{-\Lambda}^{\Lambda} \frac{d^4q}{(2\pi)^4} D_s(q) \Gamma_2(-p, q) D_H(q - p)
\end{aligned} \tag{3}$$

$$\begin{aligned}
D_s^{-1}(p) = & (1 + A)p^2 + m_s^2(1 + A) + 2(1 + A)(1 + \alpha)(1 + a)\sigma_s + \\
& (\lambda_1 + C_1) \int_{-\Lambda}^{\Lambda} \frac{d^4q}{(2\pi)^4} D_h(q) \Gamma_1(q, -p) D_h(q - p) + \\
& (\lambda_2 + C_2) \int_{-\Lambda}^{\Lambda} \frac{d^4q}{(2\pi)^4} D_H(q) \Gamma_2(q, -p) D_H(q - p)
\end{aligned} \tag{4}$$

⁵The implimentation of renormalization procedure differs from commonly used approaches in order to accommodate the intended computations.

⁶The renormalization procedure is adopted to facilitate the imposed the renormalization conditions.

where the following definitions are used:

$$\beta = \alpha m_h^2 + 2(1+A)(1+\alpha)(1+a)\sigma_h \quad (5a)$$

$$b = \alpha m_H^2 + 2(1+A)(1+\alpha)(1+a)\sigma_H \quad (5b)$$

$$B = A m_s^2 + 2(1+A)(1+\alpha)(1+a)\sigma_s \quad (5c)$$

σ_h , σ_H , σ_s are the terms to be determined during a computation. Due to their nature, above definitions do not impose any additional constraints on the equations. The definition of the two vertices during computations is given below:

$$\Gamma_1(u, v) = (1+A)(1+\alpha)(1+a)\tilde{\Gamma}_1(u, v) \quad (6a)$$

$$\Gamma_2(u, v) = (1+A)(1+\alpha)(1+a)\tilde{\Gamma}_2(u, v) \quad (6b)$$

Hence, the DSEs for the three field propagators become

$$D_h^{-1}(p) = (1+\alpha) \left[p^2 + \frac{m_{h,r}^2}{(1+\alpha)} + (\lambda_1 + C_1)(1+A)(1+a) \int_{-\Lambda}^{\Lambda} \frac{d^4 q}{(2\pi)^4} D_s(q) \tilde{\Gamma}_1(-p, q) D_h(q-p) \right] \quad (7)$$

$$D_H^{-1}(p) = (1+a) \left[p^2 + \frac{m_{H,r}^2}{1+a} + (\lambda_2 + C_2)(1+A)(1+\alpha) \int_{-\Lambda}^{\Lambda} \frac{d^4 q}{(2\pi)^4} D_s(q) \tilde{\Gamma}_2(-p, q) D_H(q-p) \right] \quad (8)$$

$$D_s^{-1}(p) = (1+A) \left[p^2 + m_s^2 + 2(1+a)(1+\alpha)\sigma_s + (\lambda_1 + C_1)(1+a)(1+\alpha) \int_{-\Lambda}^{\Lambda} \frac{d^4 q}{(2\pi)^4} D_h(q) \tilde{\Gamma}_1(q, -p) D_h(q-p) + (\lambda_2 + C_2)(1+a)(1+\alpha) \int_{-\Lambda}^{\Lambda} \frac{d^4 q}{(2\pi)^4} D_H(q) \tilde{\Gamma}_2(q, -p) D_H(q-p) \right] \quad (9)$$

where in equation 7 the renormalized mass for the SM Higgs ($m_{h,r}$) is fixed at 125.09 GeV during the entire study, while the renormalized mass of the second Higgs boson is fixed during each computation⁷. Equations 7-9 are the three DSEs considered for the study. The quantities $\tilde{\Gamma}_1(u, v)$ and $\tilde{\Gamma}_2(u, v)$ are fixed at λ_1 and λ_2 , respectively [53]. However, in the current investigation the vertices can still change depending upon the contributions from the coefficients in the counter terms, see equations 6.

In our investigation, the dynamical renormalized (squared) scalar mass is defined as the renormalized (squared) mass with insignificant contribution

⁷The definition of the squared physical mass of the SM Higgs is $m_{h,r}^2 = m_h^2 + \beta$, and the definition of the squared renormalized mass of the second Higgs is $m_{H,r}^2 = m_H^2 + b$.

from the corresponding bare mass value. The definition and the method of counter terms involving scalar mass are not in tension. It has been observed that a numerically insignificant value of the scalar bare mass does not influence any outcome. Hence, setting m_s to 0 is found equivalent for computations. During the computations, $m_s = 10^{-8}$ GeV is used.

For each of the propagators, the following renormalization conditions are used.

$$D_h^{ij}(p)|_{p^2=m_{h,r}^2} = \frac{\delta^{ij}}{p^2 + m_{h,r}^2}|_{p^2=m_{h,r}^2} \quad (10)$$

$$D_H^{ij}(p)|_{p^2=m_{H,r}^2} = \frac{\delta^{ij}}{p^2 + m_{H,r}^2}|_{p^2=m_{H,r}^2} \quad (11)$$

$$D_s(p)|_{p=1} = \frac{1}{p^2}|_{p=1} \quad (12)$$

The following two conditions are aimed to extract the correlation functions and the other quantities which are introduced for the counter terms.

$$\begin{aligned} \int_{-\Lambda}^{\Lambda} (-D_h^{-1}(p) + (1+\alpha)[p^2 + \frac{m_{h,r}^2}{(1+\alpha)} + (\lambda_1 + C_1)(1+A)(1+a) \\ \int_{-\Lambda}^{\Lambda} \frac{d^4 q}{(2\pi)^4} D_s(q) \tilde{\Gamma}_1(-p, q) D_h(q-p)])^2 dp = 0 \end{aligned} \quad (13)$$

$$\begin{aligned} \int_{-\Lambda}^{\Lambda} (-D_H^{-1}(p) + (1+a)[p^2 + \frac{m_{H,r}^2}{1+a} + (\lambda_2 + C_2)(1+A)(1+\alpha) \\ \int_{-\Lambda}^{\Lambda} \frac{d^4 q}{(2\pi)^4} D_s(q) \tilde{\Gamma}_2(-p, q) D_H(q-p)])^2 dp = 0 \end{aligned} \quad (14)$$

Equations 13 - 14 are indeed the implementation of the least square method with errors E_1 and E_2 defined below.

$$\begin{aligned} E_1 = \int_{-\Lambda}^{\Lambda} (-D_h^{-1}(p) + (1+\alpha)[p^2 + \frac{m_{h,r}^2}{(1+\alpha)} + (\lambda_1 + C_1)(1+A)(1+a) \\ \int_{-\Lambda}^{\Lambda} \frac{d^4 q}{(2\pi)^4} D_s(q) \tilde{\Gamma}_1(-p, q) D_h(q-p)])^2 dp \end{aligned} \quad (15)$$

$$\begin{aligned} E_2 = \int_{-\Lambda}^{\Lambda} (-D_H^{-1}(p) + (1+a)[p^2 + \frac{m_{H,r}^2}{1+a} + (\lambda_2 + C_2)(1+A)(1+\alpha) \\ \int_{-\Lambda}^{\Lambda} \frac{d^4 q}{(2\pi)^4} D_s(q) \tilde{\Gamma}_2(-p, q) D_H(q-p)])^2 dp \end{aligned} \quad (16)$$

With imposition of these constraints, the problem at hand becomes that of optimization in which solutions are sought which satisfy equations 13-14.

An additional condition given below is also imposed in order to ensure positivity of the renormalized squared dynamical scalar mass and evade unwanted numerical fluctuations which may arise due to the difference between the fixed renormalized masses and the dynamically generated masses, and the ever-present limitation in momentum resolution.

$$m_{s,r}^2 = (1 + A)(m_s^2 + 2(1 + \alpha)(1 + a)\sigma_s) \geq 0 \quad (17)$$

In order to further suppress numerical fluctuations, the SM Higgs is expanded in the form given below:

$$D_h^{ij}(p) = \delta^{ij} \frac{1}{c(p^2 + d + f(p))} \quad (18)$$

with $f(p)$ given by

$$f(p) = \frac{\sum_{l=0}^N a_l p^{2l}}{\sum_{l=0}^N b_l p^{2l}} \quad (19)$$

In equations 18-19, c , d , a_l , and b_l are the coefficients to be determined during a computation. A similar expansion with different coefficients is used for the second Higgs propagator. Beside stability, these expansions are also time efficient while performing renormalization and updating the SM and the second Higgs propagators.

The computation starts with $\sigma_H = \sigma_s = C_1 = C_2 = 0$, i.e. with no contribution by the counter terms to the renormalized masses and the two Yukawa couplings. Both Higgs propagators are also rendered their respective tree level structures. For the SM Higgs in equations 18-19, $c = 1$ and $d = m_h^2$ ⁸ while all the other coefficients are zero. A similar setup of coefficients is used for the second Higgs with $d = m_H^2$. The terms $1 + \alpha$ and $1 + a$ are calculated from the renormalization conditions in equations 10 and 11. The scalar propagator assumes the values using the equation 4 and the quantity $1 + A$ is calculated by the renormalization condition 12⁹.

An iteration involves updating of the correlation functions and parameters. During an iteration, first, the σ_s , C_1 , and C_2 are updated as in the mentioned ordered. The update of each of these quantities is performed using Newton Raphson's method with the criteria imposed by the least square method in equations 13-14. The updated value is accepted only when both of the errors E_1 and E_2 reduce, see equations 15-16.

⁸ $m_h^2 = m_{h,r}^2$ is used throughout the study.

⁹The scalar propagator is calculated without the term $1 + A$ and then then renormalization condition sets the value of the term $1 + A$.

It is followed by the SM Higgs propagator for which the coefficients in equations 18-19 are updated with the above mentioned criteria of acceptance. Upon each change, the SM Higgs propagator is calculated from equations 18-19 and renormalized using equation 10.

Lastly, the second Higgs propagator is updated using the same procedure as described above for the SM Higgs, but using equation 11 for renormalization. Upon every change, the scalar propagator is calculated from equation 9 and renormalized using equation 12, as mentioned earlier.

A computation concludes only when there are either no further improvements in the quantities such that E_1 and E_2 are further reduced, or both of these errors are equal or below the preset value of tolerance. The value of tolerance is set at 10^{-20} .

Gauss quadrature algorithm is used for numerical integration in the DSEs. The algorithms are developed in C++ environment.

The solutions presented are unique in the sense that order of updates performed on the propagators and other quantities practically does not effect the quantities being computed.

As the Lagrangian of the model does not contain quartic self interactions it is assumed that the model is a non-trivial theory [55–62].

The assumption that the considered model may be a part of a larger new scalar sector, containing further interaction vertices, is justifiable. As other vertices may also contribute in physical processes, the effects of the Yukawa vertices rendering the complete theory Hamiltonian negative are expected to be at least significantly mitigated even before a full theory containing the SM is considered. Hence, from the perspective of path integral approach [54], the questionable feature of negative Hamiltonian for certain paths is entirely neglected at this point. It is important to note that the large magnitude of the (squared) Higgs mass may already contribute in mitigating the effects.

Once the scalar dynamical masses in the parameter space are calculated, knowledge from machine learning [46] is employed to represent the results in an attempt to understand how scalar dynamical masses manifest in the parameter space and either estimate or impose bounds on the critical coupling value. An obvious advantage is the availability of the quantities for richer field theories which mostly require truncations and ansatz in DSE related studies. There are three free parameters in the model. Hence, scalar dynamical mass is expanded in terms of the second Higgs mass m_H , and the two Yukawa couplings (λ_1 and λ_2) as given below:

$$m_{s,f}(m_H, \lambda_1, \lambda_2) = \sum_{i=0}^{i=6} \sum_{j=0}^{j=6} \sum_{k=0}^{k=6} a_{ijk} m_H^i \lambda_1^j \lambda_2^k \quad (20)$$

where $m_{s,f}$ is the function representing scalar dynamical mass in the pa-

parameter space. The error value E_f is described by the following expression:

$$E_f = \frac{1}{N} \sqrt{\sum_{i=1}^{i=N} (m_{s,r} - m_{s,f})_i^2} \quad (21)$$

where N is the number of explored points in the parameter space and i represents the i^{th} point in the parameter space. The model is studied on 64 points for each of the cutoff values set at 10 TeV and 100 TeV. Due to the combination of cutoff effects and numerical artifacts, (supervised) machine learning [46] is performed separately at the two cutoff values.

The training proceeds as follows: The starting value of all weights a_{ijk} are set to zero which results in non-zero cost function E_f due to non-vanishing $m_{s,r}$. Against each value of i , j , and k , the weights are systematically updated using Newton Raphson method¹⁰ and a new value of E_f is computed against the update of each a_{ijk} . The update is accepted if E_f decreases for a combination of i , j , and k . If it does not, the update is reverted in favor of the previous value of a_{ijk} , and the weight for another combination of i , j , and k is considered. An iteration is complete once all intended combinations of i , j , and k are exhausted. The tolerance is set at the value 10^{-16} . The computation is concluded once the improvement of E_f is either smaller than the tolerance value, or $E_f \leq 10^{-16}$ is reached. Throughout the training, $0 \leq m_{s,f}(m_H, \lambda_1, \lambda_2)$ is imposed. In order to remove any personal bias, no value of scalar dynamical mass was taken as outliers.

Once the training is accomplished, estimates on the critical coupling value are made.

3 Field Propagators

Unlike the modelled vertices, the field propagators receive momentum dependent contributions due to Yukawa interactions while conforming to the renormalization conditions in the model¹¹. These contributions are relatively more diverse for scalar propagators as they receive contributions from both Higgs propagators due to the two interactions. However, it may also introduce numerical fluctuations induced by the two Higgs propagator DSEs as well as other involved quantities in the model.

The cutoff effects are not significant in the SM Higgs propagators throughout the explored parameter space, see figures 1-2, particularly for $\lambda_1 < 1$. The deviations are mostly due to the multiplicative constant which is computed using the renormalization condition 10. In the parameter space with

¹⁰It was found that other methods, such as bisection method, leads to numerically similar results.

¹¹The vertex may depend upon the parameters (couplings and bare mass) at most, see equation 6.

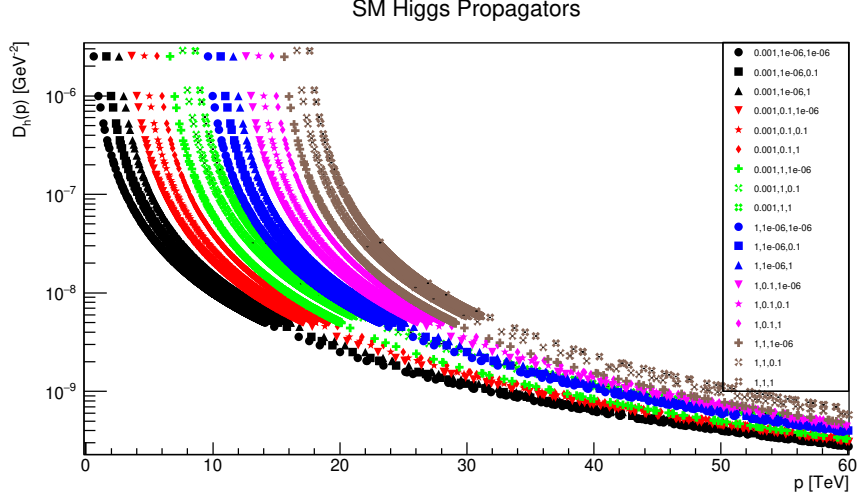


Figure 1: The SM Higgs propagators with $m_H = 0.001$ GeV and $m_H = 1.0$ GeV are plotted for cutoff values at 10 TeV and 100 TeV. The parameters in the legend are given as $(m_H, \lambda_1, \lambda_2)$ with all of the parameters mentioned in GeV. For the same cutoff, every two consecutive propagators are 1.0 TeV apart on the momentum axis for the sake of clarity.

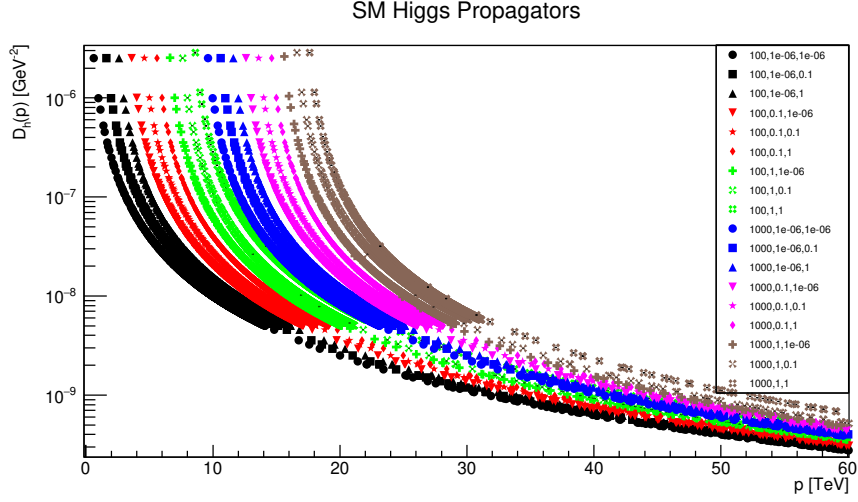


Figure 2: The SM Higgs propagators with $m_H = 100$ GeV and $m_H = 1000$ GeV are plotted for cutoff values at 10 TeV and 100 TeV. The parameters in the legend are given as $(m_H, \lambda_1, \lambda_2)$ with all of the parameters mentioned in GeV. For the same cutoff, every two consecutive propagators are 1.0 TeV apart on the momentum axis for the sake of clarity.

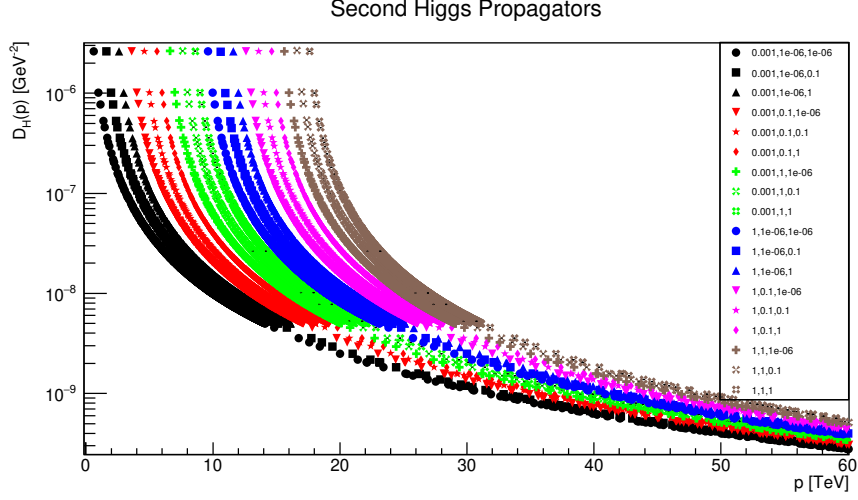


Figure 3: The second Higgs propagators with $m_H = 0.001$ GeV and $m_H = 1.0$ GeV are plotted for cutoff values at 10 TeV and 100 TeV . The parameters in the legend are given as $(m_H, \lambda_1, \lambda_2)$ with all of the parameters mentioned in GeV . For the same cutoff, every two consecutive propagators are 1.0 TeV apart on the momentum axis for the sake of clarity.

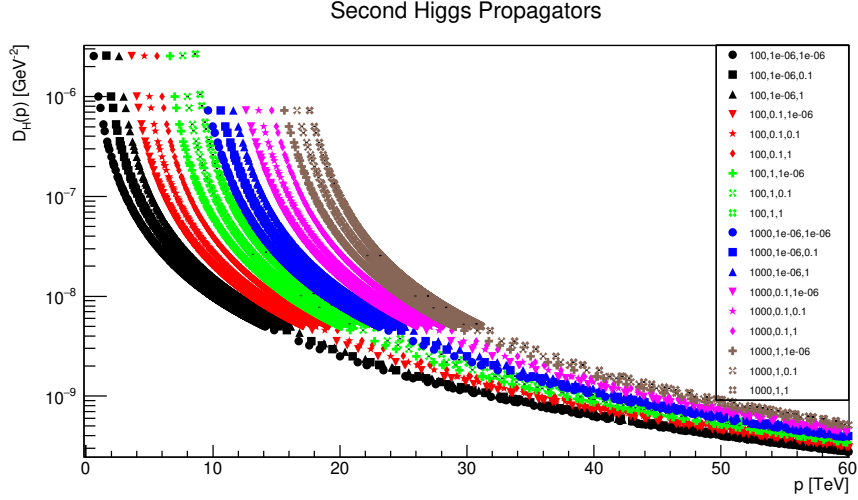


Figure 4: The second Higgs propagators with $m_H = 100$ GeV and $m_H = 1000$ GeV are plotted for cutoff values at 10 TeV and 100 TeV . The parameters in the legend are given as $(m_H, \lambda_1, \lambda_2)$ with all of the parameters mentioned in GeV . For the same cutoff, every two consecutive propagators are 1.0 TeV apart on the momentum axis for the sake of clarity.

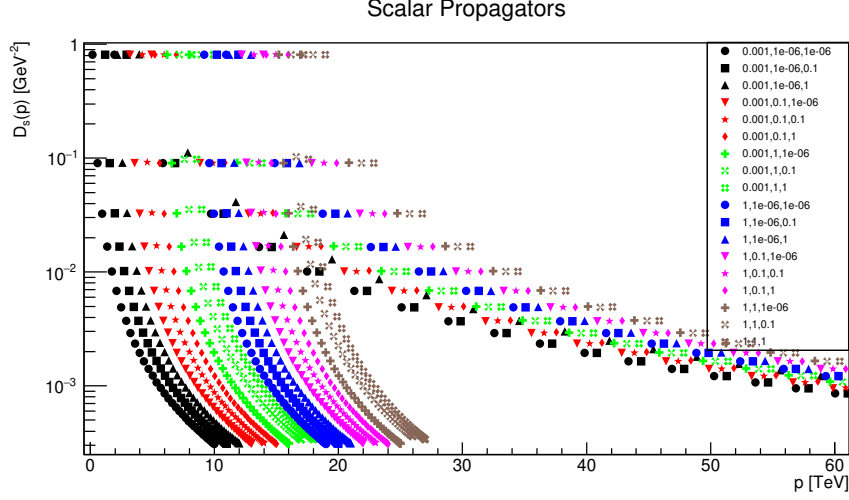


Figure 5: The scalar propagators with $m_H = 0.001$ GeV and $m_H = 1.0$ GeV are plotted for cutoff values at 10 TeV and 100 TeV. The parameters in the legend are given as $(m_H, \lambda_1, \lambda_2)$ with all of the parameters mentioned in GeV. For the same cutoff, every two consecutive propagators are 1.0 TeV apart on the momentum axis for the sake of clarity.

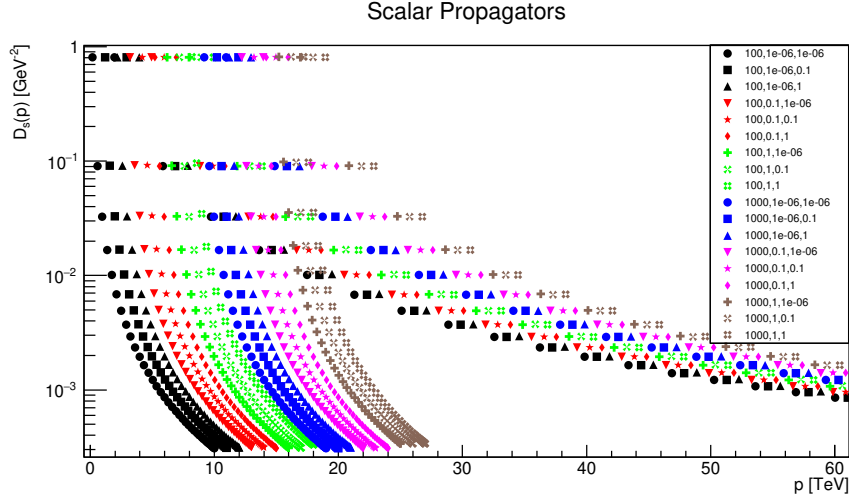


Figure 6: The scalar propagators with $m_H = 100$ GeV and $m_H = 1000$ GeV are plotted for cutoff values at 10 TeV and 100 TeV. The parameters in the legend are given as $(m_H, \lambda_1, \lambda_2)$ with all of the parameters mentioned in GeV. For the same cutoff, every two consecutive propagators are 1.0 TeV apart on the momentum axis for the sake of clarity.

λ_1 as low as 10^{-6} , the propagator is least sensitive. As the couplings are increased, slight enhancement is observed while considerable changes occur only at $\lambda_1 = 1.0$. The propagators are found to have similar qualitative behavior for all the renormalized masses of the second Higgs which indicates that the second Higgs field does not influence the SM propagators which could have been possible through the DSE of the scalar propagator. Overall, there is no significant changes in the SM Higgs propagators in the parameter space of the model.

The second Higgs field differs from the SM Higgs field due to different renormalized masses and couplings. Hence, particularly for masses in the vicinity of the SM Higgs mass, it is expected to have similar behavior within numerical fluctuations. The propagators are shown in figures 3-4. There are no considerable cutoff effects, as is the case with the SM Higgs propagators. However, a certain dependence on m_H is observed in the propagators which is relatively stronger for $m_H < m_h$ and weakens as m_H approaches m_h . The two Higgs propagators have similar behavior for $m_H \simeq m_h$ which also verifies implementation of the algorithms. For $m_H = 1$ TeV dependence on couplings is lost since the bare mass of the second Higgs field dominates in contribution to the propagators rendering it practically a tree level structure up to the renormalization dependent term. The propagators are relatively suppressed in the low momentum region for larger bare mass which is expected for the case of dominant tree level contribution to the propagator.

The scalar singlet propagators are shown in figures 5-6. As argued above, cutoff effects are evident on the propagators¹². The overall behavior is that for higher couplings, particularly λ_2 since m_h is kept fixed, the propagators are enhanced depending upon the second Higgs mass m_H . As m_H increases, this effect tends to disappear in favor of a tree level structure, as is the case for the other field propagators. The scalar propagators suffer strongly from the cutoff effects despite that both Higgs propagators are not effected to such an extent. It implies that the cutoff effects must show up in at least one of the calculated quantities other than the two Higgs propagators. The field propagators are found monotonically decreasing and without containing any peculiarities such as zero crossing.

4 Dynamical Scalar Masses

Since the scalar propagator also contains its dynamically generated mass, the arguments related to the cutoff effects and numerical artifacts translate into the dynamical masses. However, there are certain vivid features in the masses shown in the figures 7-8.

¹²There may also be contributions from the numerical interpolation performed during renormalization of the scalar propagators. In order to suppress these effects, resolution in momentum is kept at its highest, given the available resources.

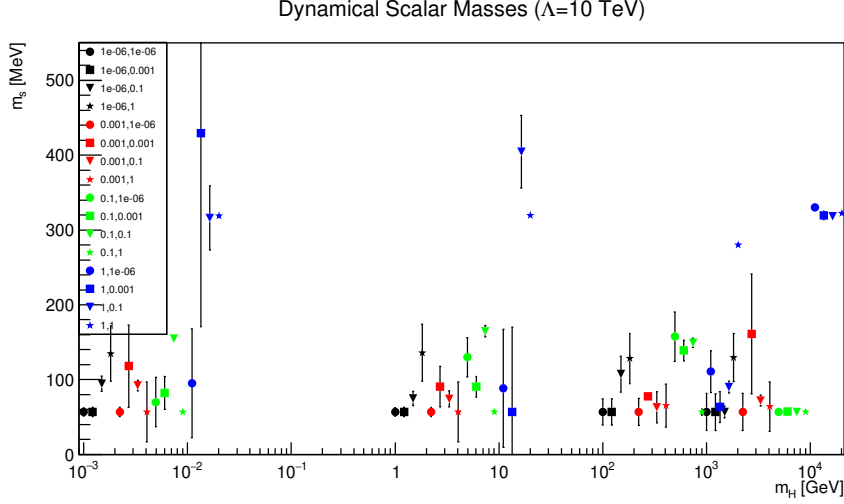


Figure 7: Dynamical scalar masses are plotted against second Higgs mass m_H for various couplings at 10 TeV cutoff. The couplings (in GeV) are shown in the caption as λ_1, λ_2 . Every consecutive pair of couplings is slightly displaced along x-axis for clarity. The error bars represent difference between the values of scalar dynamical masses obtained by computation (plotted values) and by training of the algorithms.

Considering the dynamical masses for 100 TeV cutoff in figure 8, the extent of the mass production is relatively higher for the second Higgs mass in MeVs and high second coupling for a number of cases. For very small couplings, large difference between the computed value and $m_{s,f}$, possibly due to numerical fluctuations, suggests that these two points could have been taken as outliers. Hence, it is concluded with confidence that the dynamically generated scalar mass in the model is restricted well within 200 MeVs. It is clear that the Yukawa interaction in the scalar sector has a limitation when it comes to producing dynamical masses in GeVs.

It is also evident from figures 7-8 that cutoff effects are weaker for the cutoff in hundreds of TeVs. For higher cutoff, the model produces scalar masses with less dependence on the second Higgs mass. Furthermore, the production of scalar mass is significantly lower if one of the couplings is as low as 10^{-6} GeV, unless the other coupling reaches 1.0 GeV, see figure 8. Hence, the model does possess a demarcation over the coupling values in the vicinity of 1.0 and 10^{-6} GeV. For the case of both couplings at 10^{-6} GeV, scalar mass practically loses dependence on the two couplings. It is taken as a sign of existence of critical coupling value between 10^{-3} GeV and 10^{-6} GeV.

An interesting feature in the low coupling region is that for higher cutoff values the model produces smaller masses which also tend to decrease with

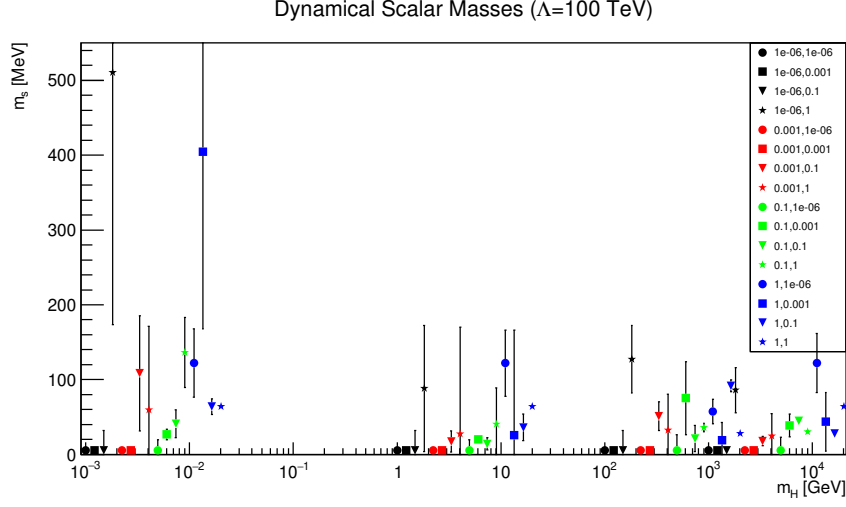


Figure 8: Dynamical scalar masses are plotted against second Higgs mass m_H for various couplings at 100 TeV cutoff. The couplings (in GeV) are shown in the caption as λ_1, λ_2 . Every consecutive pair of couplings is slightly displaced along x-axis for clarity. The error bars represent difference between the values of scalar dynamical masses obtained by computation (plotted values) and by training of the algorithms.

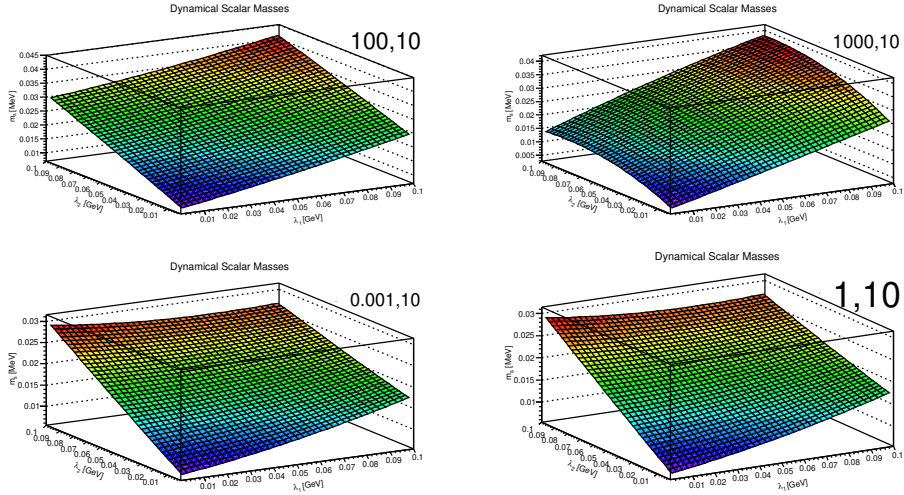


Figure 9: Dynamical scalar masses obtained by training algorithms are shown against the two couplings λ_1 and λ_2 , for various second Higgs masses m_H in GeV and at cutoff $\Lambda = 10$ TeV indicated on the caption.

the two couplings. One may expect that the behavior persists until the critical coupling value. If this is indeed the case, the model may be useful

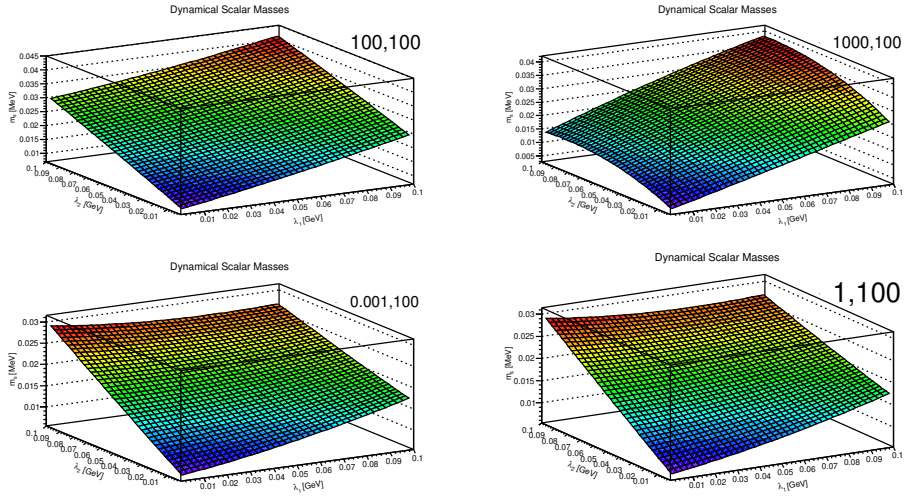


Figure 10: Dynamical scalar masses obtained by training algorithms are shown against the two couplings λ_1 and λ_2 , for various second Higgs masses m_H in GeV and at cutoff $\Lambda = 100$ TeV indicated on the caption.

to study ultralight scalar interactions [33–40], though it may undoubtedly be a daunting task from the perspective of numerical precision.

Scalar dynamical masses obtained by a trained algorithm are plotted in figures 9-10. The weights of the expansion in equation 20 are given in appendix A. An immediate observation is an indication of a unique value of the critical coupling in the model below 10^{-3} GeV. Determining exact value is hampered by the ever-present limitation associated with data and precision in machine learning. However, it is evident that the model strongly favors a critical coupling in the region $10^{-6} < \lambda_i < 10^{-3}$ GeV.

However, the weights a_{ijk} are found to have a particular behavior. Firstly there are strong contributions from the terms with $k = 0$ and $i, j \neq 0$, while there is practically no contributions from a_{ijk} for $i, j = 0$ irrespective of the value of k . Increasing the cutoff suppresses a_{ijk} for most of the i and k values at $j = 0$. Since the model has significant cutoff effects which become milder as the cutoff is raised, it is expected that scalar dynamical mass may not receive significant contributions from the terms involving $j = 0$ at high cutoff values.

5 Conclusion

In the presence of an SM Higgs, the two Higgs doublet model has the capacity to dynamically produce scalar masses in the vicinity of, or even larger than, that of the lightest leptons or quarks. As the cutoff is raised above 100 TeV, stability in the mass with magnitude below 200 MeV ensues against

the second Higgs mass. However, the dynamical mass has sensitivity to the couplings which diminishes as the couplings are reduced below 10^{-3} GeV, with the minimum mass being produced. It strongly points towards existence of a critical coupling between 10^{-3} GeV and 10^{-6} GeV. It presents an opportunity to investigate the model to understand new physics involving the particles considerably lighter than 1 GeV, such as ultra-light scalars. At the same time, it invites for further study of richer models which contain higher renormalizable vertices in an attempt to explore existence of critical couplings and extent of mass generation in the presence of variety of interactions.

The role of cutoff effects can not be neglected in the model. Scalar propagator and scalar dynamical mass suffer the most, while for (both) Higgs masses larger than 100 GeV the field propagators are relatively less effected as was observed in the two Higgs propagators. Since dynamical masses are less than 1 GeV, numerical fluctuations and the cutoff effects hamper in finding an accurate description of how the masses behave in the parameter space. However, considering sufficient number of points in the parameter space a mathematical description for dynamical masses was still found which concurs with the deduction regarding the critical coupling in the model.

A model with the capacity to dynamically produce masses considerably larger than the lightest quarks and leptons can certainly not be ruled out in scalar interactions. The study invites extensions, such as by including richer interactions or other fields, to have a better understanding of how (particularly light) scalars play role at the fundamental level in our universe.

6 Acknowledgments

This work was supported by Lahore University of Management Sciences, Pakistan for developing the algorithms and performing computations.

7 Appendix A

The values of the weights a_{ijk} in equation 20 for cutoff values at $\Lambda = 10$ TeV and $\Lambda = 100$ TeV are given below:

i	j	k	a_{ijk} (10 TeV)	a_{ijk} (100 TeV)
0	0	0	0.062470119000000	-0.005102152199999
1	0	0	0.432639286999998	0.067154687499999
0	1	0	0.431424060300000	0.276498992400000
0	0	1	0.000127544300000	0.000023271900000
2	0	0	-0.196267245799999	0.826964182800007

1	1	0	3.483278381999988	-2.646594633199990
1	0	1	0.001256076799999	0.000786048000000
0	2	0	-2.426385300799987	-0.005208820599999
0	1	1	-0.001780857000000	-0.000014844700000
0	0	2	-0.0000001083	-0.000000023100000
3	0	0	-0.595301560000001	-0.158007649599999
2	1	0	0.311572103699999	5.428065021000011
2	0	1	-0.001414899099999	-0.002876003599999
1	2	0	-2.967471651800008	-3.556474306000007
1	1	1	-0.011901846299999	0.013548386599999
1	0	2	-0.0000018441	-0.000000603000000
0	3	0	3.360127912999990	-0.928262618399999
0	2	1	0.004300518299999	-0.002201626699999
0	1	2	0.000000999000000	-0.000000020900000
0	0	3	0.0	0.0
4	0	0	1.045801962500008	-0.402565733399999
3	1	0	-1.420411216799999	-0.572378273000001
3	0	1	0.003927822499999	-0.000554230599999
2	2	0	-1.122774422700004	-0.529377973400000
2	1	1	0.000976498800000	-0.005964260699999
2	0	2	0.0000004915	0.000001401500000
1	3	0	0.322474038600001	3.267544194000007
1	2	1	0.005696769799999	-0.001591530000000
1	1	2	0.0000093254	-0.000008751100000
1	0	3	0.0	0.0
0	4	0	-3.398481779199986	1.658322491499994
0	3	1	-0.002802221199999	0.001725826300000
0	2	2	-0.0000000495	0.000000259100000
0	1	3	0.0	0.0
0	0	4	0.0	0.0
5	0	0	-0.831871660400005	0.132814269100000
4	1	0	0.949120657999995	-1.788138425800004
4	0	1	-0.003439259299999	0.001322541799999
3	2	0	-1.903333068200005	-4.520240236500010
3	1	1	-0.005681518600000	0.006113348800000
3	0	2	0.0000018543	0.000000118100000
2	3	0	5.737533950000011	2.994909360000007
2	2	1	0.004100454999999	-0.003434122199999
2	1	2	0.0000045994	-0.000004740900000
2	0	3	0.0	0.0
1	4	0	-4.607335835299982	3.560205072699987

1	3	1	-0.0017640611	0.000632370000000
1	2	2	-0.000002936	0.000001718100000
1	1	3	0.0	0.0
1	0	4	0.0	0.0
0	5	0	2.476695333800004	-1.438056151699995
0	4	1	-0.001170340799999	0.000608526900000
0	3	2	-0.0000001277	0.000000238100000
0	2	3	0.0	0.0
0	1	4	0.0	0.0
0	0	5	0.0	0.0
6	0	0	0.250543694400000	-0.303845693199999
5	1	0	-0.872865771300006	-0.570790623500001
5	0	1	-0.0014202491	-0.000099293799999
4	2	0	-2.629992650700005	-4.544265494000010
4	1	1	-0.002726043499999	0.004424348300000
4	0	2	0.0000007263	0.000000419100000
3	3	0	4.539023046400008	-1.631924930300001
3	2	1	0.004210737	0.000127814799999
3	1	2	0.0000038225	-0.000004546200000
3	0	3	0.0	0.0
2	4	0	-2.361741260400014	7.959941882000007
2	3	1	0.0004258372	-0.003437821899999
2	2	2	-0.0000105292	0.000010411400000
2	1	3	0.0	0.0
2	0	4	0.0	0.0
1	5	0	2.65929292970001	-3.122536580600026
1	4	1	0.007337953699999	-0.008389909299999
1	3	2	-0.0000050914	0.000004083200000
1	2	3	0.0	0.0
1	1	4	0.0	0.0
1	0	5	0.0	0.0
0	6	0	-0.408070357499999	0.605073464699998
0	5	1	0.0012935581	-0.001141694000000
0	4	2	-0.0000006819	0.000000429700000
0	3	3	0.0	0.0
0	2	4	0.0	0.0
0	1	5	0.0	0.0
0	0	6	0.0	0.0

References

- [1] Tomas Brauner and Jiri Hosek. Dynamical fermion mass generation by a strong Yukawa interaction. *Phys. Rev.*, D72:045007, 2005.
- [2] Pieter Maris and Peter C. Tandy. Bethe-Salpeter study of vector meson masses and decay constants. *Phys. Rev.*, C60:055214, 1999.
- [3] Christian S. Fischer and Reinhard Alkofer. Nonperturbative propagators, running coupling and dynamical quark mass of Landau gauge QCD. *Phys. Rev.*, D67:094020, 2003.
- [4] A. C. Aguilar, A. V. Nesterenko, and J. Papavassiliou. Infrared enhanced analytic coupling and chiral symmetry breaking in QCD. *J. Phys.*, G31:997, 2005.
- [5] Patrick O. Bowman, Urs M. Heller, Derek B. Leinweber, Maria B. Parappilly, Anthony G. Williams, and Jian-bo Zhang. Unquenched quark propagator in Landau gauge. *Phys. Rev.*, D71:054507, 2005.
- [6] A. C. Aguilar and J. Papavassiliou. Chiral symmetry breaking with lattice propagators. *Phys. Rev.*, D83:014013, 2011.
- [7] Ian C. Cloet and Craig D. Roberts. Explanation and Prediction of Observables using Continuum Strong QCD. *Prog. Part. Nucl. Phys.*, 77:1–69, 2014.
- [8] Mario Mitter, Jan M. Pawłowski, and Nils Strodthoff. Chiral symmetry breaking in continuum QCD. *Phys. Rev.*, D91:054035, 2015.
- [9] Daniele Binosi, Lei Chang, Joannis Papavassiliou, Si-Xue Qin, and Craig D. Roberts. Natural constraints on the gluon-quark vertex. *Phys. Rev.*, D95(3):031501, 2017.
- [10] Alejandro Ayala, Adnan Bashir, Alfredo Raya, and Eduardo Rojas. Dynamical mass generation in strongly coupled quantum electrodynamics with weak magnetic fields. *Phys. Rev.*, D73:105009, 2006.
- [11] M. V. Libanov and V. A. Rubakov. More about spontaneous Lorentz-violation and infrared modification of gravity. *JHEP*, 08:001, 2005.
- [12] Petr Benes, Tomas Brauner, and Adam Smetana. Dynamical electroweak symmetry breaking due to strong Yukawa interactions. *J. Phys.*, G36:115004, 2009.
- [13] John M. Cornwall. Dynamical Mass Generation in Continuum QCD. *Phys. Rev. D*, 26:1453, 1982.
- [14] J. Beringer et al. (Particle Data Group). *Phys. Rev. D*, 86:010001, 2012.

- [15] Marcela Carena and Howard E. Haber. Higgs boson theory and phenomenology. *Prog. Part. Nucl. Phys.*, 50:63–152, 2003.
- [16] Georges Aad et al. Observation of a new particle in the search for the Standard Model Higgs boson with the ATLAS detector at the LHC. *Phys. Lett.*, B716:1–29, 2012.
- [17] Serguei Chatrchyan et al. Observation of a new boson at a mass of 125 GeV with the CMS experiment at the LHC. *Phys. Lett.*, B716:30–61, 2012.
- [18] M. Malbertion. SM Higgs boson measurements at CMS. *Nuovo Cim.*, C40(5):182, 2018.
- [19] Fedor Bezrukov and Abigail Keats. Light inflaton model in a metastable universe. *Phys. Rev. D*, 104(7):075020, 2021.
- [20] Fedor Bezrukov. The Higgs field as an inflaton. *Class. Quant. Grav.*, 30:214001, 2013.
- [21] V. Mukhanov. *Physical Foundations of Cosmology*. Cambridge University Press, Oxford, 2005.
- [22] Jae-Weon Lee. Brief History of Ultra-light Scalar Dark Matter Models. *EPJ Web Conf.*, 168:06005, 2018.
- [23] M. C. Bento, O. Bertolami, R. Rosenfeld, and L. Teodoro. Selfinteracting dark matter and invisibly decaying Higgs. *Phys. Rev.*, D62:041302, 2000.
- [24] Orfeu Bertolami, Catarina Cosme, and João G. Rosa. Scalar field dark matter and the Higgs field. *Phys. Lett.*, B759:1–8, 2016.
- [25] Carlos Munoz. Models of Supersymmetry for Dark Matter. 2017. [EPJ Web Conf.136,01002(2017)].
- [26] Stephen P. Martin. A Supersymmetry primer. 1997. [Adv. Ser. Direct. High Energy Phys.18,1(1998)].
- [27] Matthew D. Schwartz. *Quantum Field Theory and the Standard Model*. Cambridge University Press, 2014.
- [28] M. Kaku. *Quantum field theory: A Modern introduction*. 1993.
- [29] Michael E. Peskin and Daniel V. Schroeder. *An Introduction to quantum field theory*. Addison-Wesley, Reading, USA, 1995.
- [30] John F. Gunion and Howard E. Haber. The CP conserving two Higgs doublet model: The Approach to the decoupling limit. *Phys. Rev.*, D67:075019, 2003.

- [31] M. E. Cabrera, J. A. Casas, A. Delgado, and S. Robles. 2HDM singlet portal to dark matter. *JHEP*, 01:123, 2021.
- [32] Wolfgang Altmannshofer, Stefania Gori, Nick Hamer, and Hiren H. Patel. Electron EDM in the complex two-Higgs doublet model. *Phys. Rev. D*, 102:115042, 2020.
- [33] Tanja Rindler-Daller and Paul R. Shapiro. Complex scalar field dark matter on galactic scales. *Mod. Phys. Lett. A*, 29(2):1430002, 2014.
- [34] Tiberiu Harko. Gravitational collapse of Bose-Einstein condensate dark matter halos. *Phys. Rev. D*, 89(8):084040, 2014.
- [35] Pierre-Henri Chavanis. Mass-radius relation of Newtonian self-gravitating Bose-Einstein condensates with short-range interactions: I. Analytical results. *Phys. Rev. D*, 84:043531, 2011.
- [36] Kerson Huang, Chi Xiong, and Xiaofei Zhao. Scalar-field theory of dark matter. *Int. J. Mod. Phys. A*, 29(13):1450074, 2014.
- [37] David J. E. Marsh. Axion Cosmology. *Phys. Rept.*, 643:1–79, 2016.
- [38] Lam Hui, Jeremiah P. Ostriker, Scott Tremaine, and Edward Witten. Ultralight scalars as cosmological dark matter. *Phys. Rev. D*, 95(4):043541, 2017.
- [39] Joel R. Primack. Cosmology: small scale issues revisited. *New J. Phys.*, 11:105029, 2009.
- [40] Wayne Hu, Rennan Barkana, and Andrei Gruzinov. Cold and fuzzy dark matter. *Phys. Rev. Lett.*, 85:1158–1161, 2000.
- [41] Jurij W. Darewych. Some exact solutions of reduced scalar Yukawa theory. *Can. J. Phys.*, 76:523–537, 1998.
- [42] Vladimir B. Sauli. Nonperturbative solution of metastable scalar models: Test of renormalization scheme independence. *J. Phys.*, A36:8703–8722, 2003.
- [43] G. V. Efimov. On the ladder Bethe-Salpeter equation. *Few Body Syst.*, 33:199–217, 2003.
- [44] E. Ya. Nugaev and M. N. Smolyakov. Q-balls in the Wick–Cutkosky model. *Eur. Phys. J.*, C77(2):118, 2017.
- [45] J. W. Darewych and A. Duviryak. Confinement interaction in nonlinear generalizations of the Wick–Cutkosky model. *J. Phys.*, A43:485402, 2010.

- [46] Ethem Alpaydin. *Introduction to Machine Learning*. MIT Press, 2014.
- [47] Dimitrios Bachtis, Gert Aarts, and Biagio Lucini. Quantum field-theoretic machine learning. *Phys. Rev. D*, 103(7):074510, 2021.
- [48] James Halverson, Anindita Maiti, and Keegan Stoner. Neural Networks and Quantum Field Theory. *Mach. Learn. Sci. Tech.*, 2(3):035002, 2021.
- [49] Tetsuya Akutagawa, Koji Hashimoto, and Takayuki Sumimoto. Deep Learning and AdS/QCD. *Phys. Rev. D*, 102(2):026020, 2020.
- [50] Julian S. Schwinger. On the Green’s functions of quantized fields. 1. *Proc. Nat. Acad. Sci.*, 37:452–455, 1951.
- [51] Julian S. Schwinger. On the Green’s functions of quantized fields. 2. *Proc. Nat. Acad. Sci.*, 37:455–459, 1951.
- [52] Eric S. Swanson. A Primer on Functional Methods and the Schwinger-Dyson Equations. *AIP Conf.Proc.*, 1296:75–121, 2010.
- [53] Craig D. Roberts and Anthony G. Williams. Dyson-Schwinger equations and their application to hadronic physics. *Prog. Part. Nucl. Phys.*, 33:477–575, 1994.
- [54] R. J. Rivers. *PATH INTEGRAL METHODS IN QUANTUM FIELD THEORY*. Cambridge University Press, 1988.
- [55] A. Hasenfratz, K. Jansen, J. Jersak, C. B. Lang, T. Neuhaus, and H. Yoneyama. Study of the Four Component ϕ^4 Model. *Nucl. Phys.*, B317:81–96, 1989.
- [56] F. Gliozzi. A Nontrivial spectrum for the trivial $\lambda\phi^4$ theory. *Nucl. Phys. Proc. Suppl.*, 63:634–636, 1998.
- [57] A. Weber, J. C. Lopez Vieyra, Christopher R. Stephens, S. Dilcher, and P. O. Hess. Bound states from Regge trajectories in a scalar model. *Int. J. Mod. Phys.*, A16:4377–4400, 2001.
- [58] Renata Jora. Φ^4 theory is trivial. *Rom. J. Phys.*, 61(3-4):314, 2016.
- [59] Michael Aizenman. Proof of the Triviality of ϕ^4 Field Theory and Some Mean-Field Features of Ising Models for $d \leq 4$. *Phys. Rev. Lett.*, 47:886–886, 1981.
- [60] Peter Weisz and Ulli Wolff. Triviality of ϕ^4 theory: small volume expansion and new data. *Nucl. Phys.*, B846:316–337, 2011.
- [61] Johannes Siefert and Ulli Wolff. Triviality of ϕ^4 theory in a finite volume scheme adapted to the broken phase. *Phys. Lett.*, B733:11–14, 2014.

- [62] Matthijs Hogervorst and Ulli Wolff. Finite size scaling and triviality of ϕ^4 theory on an antiperiodic torus. *Nucl. Phys.*, B855:885–900, 2012.